A STRING OF RADIO EMISSION ASSOCIATED WITH IRAS 16562−3959: A COLLIMATED JET EMANATING FROM A LUMINOUS MASSIVE YOUNG STELLAR OBJECT

ANDRÉS E. GUZMÁN[1], GUIDO GARAY[1], AND KATE J. BROOKS[2]

[1] Departamento de Astronomía, Universidad de Chile, Camino el Observatorio 1515, Las Condes, Santiago, Chile
[2] CSIRO Astronomy and Space Science, P.O. Box 76, Epping 1710 NSW, Australia
Received 2010 July 6; accepted 2010 October 3; published 2010 November 19

ABSTRACT

We report the discovery, made using the Australia Telescope Compact Array, of a remarkable string of radio emission toward IRAS 16562−3959, a luminous infrared source with a bolometric luminosity of $7.0 \times 10^4 \, L_\odot$. The radio emission arises from a compact, bright central component, two inner lobes which are separated by about $7''$ and symmetrically offset from the central source, and two outer lobes which are separated by about $45''$. The emission from the central object has a spectral index between 1.4 and 8.6 GHz of 0.85 ± 0.15, consistent with free–free emission from a thermal jet. The radio emission from the lobes has spectral indices in the range characteristic of thermal emission. We suggest that the emission from the lobes arises in shocks resulting from the interaction of a collimated wind with the surrounding medium. The radio string is located within a massive dense molecular core, and is associated with extended green emission (*Spitzer* three-color), Herbig–Haro-type emission (2MASS K_s band), and OH maser sites—all phenomena readily observed toward sites of massive star formation. We conclude that the massive core hosts a high-mass star in an early stage of evolution in which it is undergoing the ejection of a powerful collimated stellar wind, showing that jets found in the formation of low-mass stars are also produced in high-mass stars.

Key words: ISM: individual objects (IRAS 16562−3959) – ISM: jets and outflows – radio continuum: stars – stars: formation – stars: winds, outflows

1. INTRODUCTION

The determination whether massive stars are formed via accretion or via merging processes is one of the main observational challenges in the field of star formation. If massive O-type stars are formed by an accretion process similar to that inferred for low-mass stars, then we expect that circumstellar disks and jets will be present in their earliest stages of evolution.

To date there are only a handful of massive young stellar objects (MYSOs) known to be associated with highly collimated jets and/or Herbig–Haro (HH) objects. All except one have luminosities smaller than $2 \times 10^4 \, L_\odot$ corresponding to that of a B0 zero-age main-sequence (ZAMS) star. They include IRAS 18162−2048 ($L \sim 1.7 \times 10^4 \, L_\odot$; Martí et al. 1993), Cepheus A HW2 ($L \sim 1 \times 10^4 \, L_\odot$; Rodríguez et al. 1994), IRAS 20126+4104 ($L \sim 1.3 \times 10^4 \, L_\odot$; Cesaroni et al. 1997), G192.16−3.82 ($L \sim 3 \times 10^3 \, L_\odot$; Shepherd et al. 1998, 2001; Devine et al. 1999), and W75N, which contains several molecular and HH outflows powered by at least four late- to early-B protostars (Shepherd et al. 2003). There is only one YSO with $L > 2 \times 10^4 \, L_\odot$ that is associated with a highly collimated jet (IRAS 16547−4247, $L \sim 6.2 \times 10^4 \, L_\odot$; Garay et al. 2003; Rodríguez et al. 2005, 2008; Brooks et al. 2007). Two other luminous YSOs, IRAS 18089−1732 ($L \sim 3.2 \times 10^4 \, L_\odot$; Beuther & Walsh 2008) and G331.51−0.10 ($L \sim 1 \times 10^5 \, L_\odot$; Bronfman et al. 2008), are associated with radio continuum sources with spectral indices characteristic of collimated stellar winds, but the angular resolution of the observations is insufficient to resolve the jet/flow morphology. It is not clear whether the lack of young massive stars with spectral types earlier than B0 ZAMS associated with jets and/or disks is an intrinsic property of the most massive stars or due to observational disadvantages—massive stars are rarer and their evolutionary timescales are much shorter than those of low-mass stars.

Currently, we are carrying out a systematic search for jets toward MYSOs to assess whether or not they are a common phenomenon (A. E. Guzmán 2011, in preparation). In this paper, we report the discovery, made using the Australia Telescope Compact Array (ATCA), of a string of radio continuum emission associated with IRAS 16562−3959. Assuming that this source is located at the distance of 1.6 kpc ($V_{\mathrm{LSR}} = -12.6$ km s^{-1}; Urquhart et al. 2008b),[3] the total far-infrared (FIR) luminosity, computed using the observed *IRAS* fluxes (see Casoli et al. 1986) is $\sim 7.0 \times 10^4 \, L_\odot$. The target was selected from a list of sources compiled by us with *IRAS* luminosities in excess of $2 \times 10^4 \, L_\odot$ and radio emission much weaker than that expected from the total FIR luminosity. The expectation is that objects with these characteristics are high-mass objects in the pre-ultracompact (UC) H II region phase, in which the weak radio emission is most likely arising from stellar wind phenomena (Hoare et al. 2007). IRAS 16562−3959 was observed as part of the RMS Survey (G345.4938+01.4677; Urquhart et al. 2008a). The emission detected at 4.8 and 8.6 GHz with ATCA (Urquhart et al. 2007) was weaker than expected. Moreover, the positive radio spectral index between these two frequencies and the hint of a string of multiple sources gave us strong indications that this source could be an ionized jet associated with an MYSO.

In this paper, we present new ATCA data taken at four frequencies (1.4, 2.4, 4.8, and 8.6 GHz). Based on these data, we propose that the string of five radio sources detected toward IRAS 16562−3959 is composed of a central thermal jet, plus inner and outer lobes of shock ionized gas resulting from the interaction of the highly collimated stellar wind with the surrounding medium.

---

[3] The twofold distance ambiguity was resolved in Faúndez et al. (2004).

Table 1
Observed Parameters of Radio Sources

Source	8.6 GHz Peak Position		Flux Density (mJy)			
	α(2000)	δ(2000)	1.4 GHz	2.4 GHz	4.8 GHz	8.6 GHz
Central (C)	$16^h59^m41\overset{s}{.}63$	$-40°03'43\overset{''}{.}61$	2.0 ± 1.0	4.2 ± 0.8	8.1 ± 0.2	12.1 ± 0.2
Inner-east (I-E)	$16^h59^m41\overset{s}{.}87$	$-40°03'44\overset{''}{.}55$	5.4 ± 0.9	7.0 ± 0.7	6.3 ± 0.2	5.7 ± 0.1
Inner-west (I-W)	$16^h59^m41\overset{s}{.}35$	$-40°03'42\overset{''}{.}94$	5.3 ± 0.9	6.7 ± 0.7	5.8 ± 0.2	3.3 ± 0.2
Outer-east (O-E)	$16^h59^m44\overset{s}{.}07$	$-40°03'52\overset{''}{.}21$	9.7 ± 0.3	5.2 ± 0.2	9.0 ± 0.3	7.6 ± 0.4
Outer-west (O-W)	$16^h59^m39\overset{s}{.}83$	$-40°03'41\overset{''}{.}90$	4.0 ± 0.7	8.0 ± 0.5	6.2 ± 0.2	3.9 ± 0.3

2. OBSERVATIONS

The radio continuum observations were made using the ATCA[4] during 2008 June and October, and 2009 February. We used the 1.5B, 1.5C, and 6.0A configurations, utilizing all six antennas and covering east–west baselines from 30 m to 5.9 km. Observations were made at four frequencies: 1.384, 2.368, 4.800, and 8.640 GHz, each with a bandwidth of 128 MHz, full Stokes. Throughout this work, we will refer to these frequencies as 1.4, 2.4, 4.8, and 8.6 GHz, respectively. The phase center of the array was R.A. = $16^h59^m41\overset{s}{.}61$, decl. = $-40°03'43\overset{''}{.}4$ (J2000). The total integration time at each frequency was about 180 minutes, obtained from 10 minute scans taken over a wide range of hour angles to provide good (u, v) coverage. The calibrator PKS 1740−517 was observed for 3 minutes before and after every on-source scan in order to correct the amplitude and phase of the interferometer data for atmospheric and instrumental effects as well as to calibrate the bandpass.

The flux density was calibrated by observing PKS 1934−638 (3C84) for which values of 14.95, 11.59, 5.83, and 2.84 Jy were adopted at 1.4, 2.4, 4.8, and 8.6 GHz, respectively. Standard calibration and data reduction were performed using MIRIAD (Sault et al. 1995). Maps were made by Fourier transformation of the uniformly weighted interferometer data. The noise levels achieved in the images are 0.38, 0.21, 0.096, and 0.070 mJy beam^{-1} and the synthesized (FWHM) beams obtained were $10\overset{''}{.}23 \times 5\overset{''}{.}71$, $5\overset{''}{.}97 \times 3\overset{''}{.}27$, $2\overset{''}{.}81 \times 1\overset{''}{.}83$, and $1\overset{''}{.}62 \times 1\overset{''}{.}01$, at the frequencies of 1.4, 2.4, 4.8, and 8.6 GHz, respectively. We estimate the flux uncertainty to be approximately 20%.

3. RESULTS

Figure 1 shows maps of the radio continuum emission from IRAS 16562−3959 at the four frequencies observed with ATCA. The maps at the lower frequencies (1.4 and 2.4 GHz) show three sources roughly lying in a linear structure along a direction with position angle (P.A.) of 99°.1. The outermost sources which we will call outer-east and outer-west, labeled O-E and O-W in Figure 1, respectively, are separated by an angular distance of ∼45″ (corresponding to 0.35 pc at 1.6 kpc). The maps at the higher frequencies (4.8 and 8.6 GHz) show that the central object seen at low frequencies is resolved into three components aligned along a direction with P.A. of 98°.9. The external components of this triplet, which we will call inner-east and inner-west components (labeled I-E and I-W), are symmetrically located in opposite directions from the bright central source (labeled C) and separated by ≈7″. Throughout this work, we will use the abbreviations C, I-E, I-W, O-E, and O-W for the central, inner-east, inner-west, outer-east, and outer-west components, respectively.

We note that the five radio components are not exactly aligned, exhibiting a small bending. The lines joining the east components and the central source and the west components and the central source form an angle of 168°. We also note that in the 8.6 GHz image there are three small knots located about 4″ north from the outer-east lobe, with peak fluxes of 0.6 mJy. The knots are well aligned with the inner and central components suggesting that they could be part of a string of emission, but more sensitive observations are needed to confirm this or disprove as artifacts of the data reduction. We will not discuss these components further in this work.

The position and flux densities of all radio components detected toward IRAS 16562−3959 are given in Table 1. For all sources the flux densities were determined from Gaussian fittings using the MIRIAD task IMFIT, with the exception of the outer components at 4.8 and 8.6 GHz. For these, the flux density was measured over the 3σ contour level. To estimate the flux densities of the C, I-E, and I-W components at 1.4 and 2.4 GHz, we fitted the observed morphology with three unresolved Gaussians centered at the positions determined from the 8.6 GHz observations.

Figure 2 shows the spectral energy distribution (SED) of the integrated radio continuum emission from the five components. Also plotted in the spectra of the central component are the values reported by Urquhart et al. (2007) at 4.8 and 8.6 GHz of 4.8 and 12.5 mJy, respectively. We find that the radio continuum spectra of component C are well fitted by a power-law spectrum ($S_\nu \propto \nu^\alpha$, where S_ν is the flux density at frequency ν), with a spectral index α of 0.85 ± 0.15. For the other components, the data were fitted using a model of thermal emission from a homogeneous region of ionized gas. The parameters EM and Ω, emission measure and solid angle, respectively, are given in each panel.

4. DISCUSSION

4.1. The Nature of the Radio Sources

The spectral index of the radio continuum emission from component C, of 0.85 ± 0.15, indicates free–free emission arising from a thermal jet. Theoretical calculations show that collimated stellar winds can have spectral indices in the range 0.25–1.1 depending on the radial dependence of the physical quantities of the jet (Reynolds 1986). They also predict that the angular size depends on frequency. However, the angular resolution of our observations does not allow us to investigate this dependence and observations with higher angular resolution are needed to resolve the jet.

Assuming that the central source is a bipolar, pressure-confined jet, which has a spectral index of 0.84, Equations (13) and (19) of Reynolds (1986) yield, for a distance of 1.6 kpc and an observed flux density at 8.6 GHz of 12.1 mJy, there are the
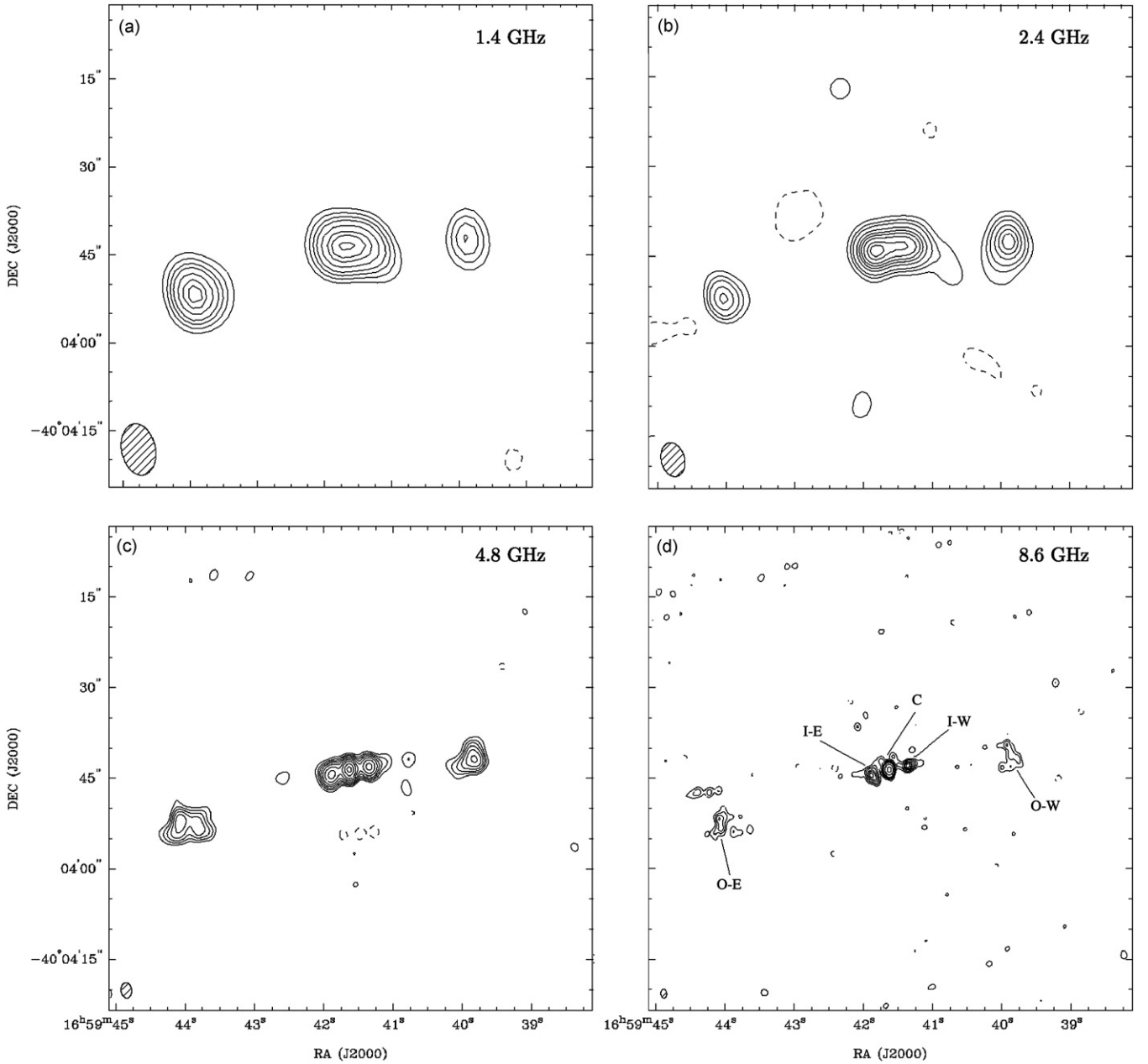
Figure 1. ATCA maps of the radio continuum emission from IRAS 16562−3959. Beams are shown in the lower left corner of each panel. Top left: 1.4 GHz map. Contour levels are −4, 4, 6, 8, 10, 13, 16, 18, and 20 times σ ($1\sigma = 0.35$ mJy beam^{-1}). Top right: 2.4 GHz map. Contour levels are −7, 7, 12, 17, 25, 32, 38, 45, 54, and 60 times σ ($1\sigma = 0.12$ mJy beam^{-1}). Bottom left: 4.8 GHz map. Contour levels are −4, 3, 6, 9, 13, 19, 28, 40, 60, and 80 times σ ($1\sigma = 0.086$ mJy beam^{-1}). Bottom right: 8.6 GHz map. Contour levels are −4, 3, 6, 9, 13, 16, 19, 24, 50, and 100 times σ ($1\sigma = 0.081$ mJy beam^{-1}).

following constraints on the jet physical parameters:

$$\left(\frac{n_{\rm jet}(r)}{10^6\,{\rm cm}^{-3}}\right) = 1.32 \left(\frac{r}{10^{-3}\,{\rm pc}}\right)^{-0.9} \left(\frac{\nu_m}{10\,{\rm GHz}}\right)^{0.818}$$
$$\times \left(\frac{\theta}{0.2}\right)^{-0.7} \left(\frac{\sin i}{\sin 45^\circ}\right)^{0.3}, \qquad (1)$$

$$\left(\frac{\dot{M}_w}{10^{-6}\,M_\odot\,{\rm yr}^{-1}}\right) = 2.8 \left(\frac{v_w}{10^3\,{\rm km\,s}^{-1}}\right) \left(\frac{\nu_m}{10\,{\rm GHz}}\right)^{0.18}$$
$$\times \left(\frac{\theta}{0.2}\right)^{3/4} \left(\frac{\sin i}{\sin 45^\circ}\right)^{-1/4}, \qquad (2)$$

where $n_{\rm jet}(r)$ is the number density of the jet at a distance r from

the MYSO, ν_m is the turnover frequency, θ is the opening angle at the base of the jet, i is the inclination angle with respect to the line of sight, v_w is the wind velocity, and $\dot{M}_w$ is the mass-loss rate. Most of these parameters are unknown. In deriving these expressions, in addition to the observational constraint, we assumed an ionization fraction of 1 and a temperature of 8000 K at the base of the jet; and a mean particle mass of $1.3 m_{\rm H}$ per hydrogen atom.

The degree of collimation of the jet source can be estimated from the size of the lobes and their distance to the central component. Using the data obtained for the east and west outer lobes, we derive that $\theta \sim 0.2$ rad. Assuming that v_w is 500 km s^{-1}, a value typical of jets associated with luminous objects (Anglada 1996; Martí et al. 1998; Curiel et al. 2006;
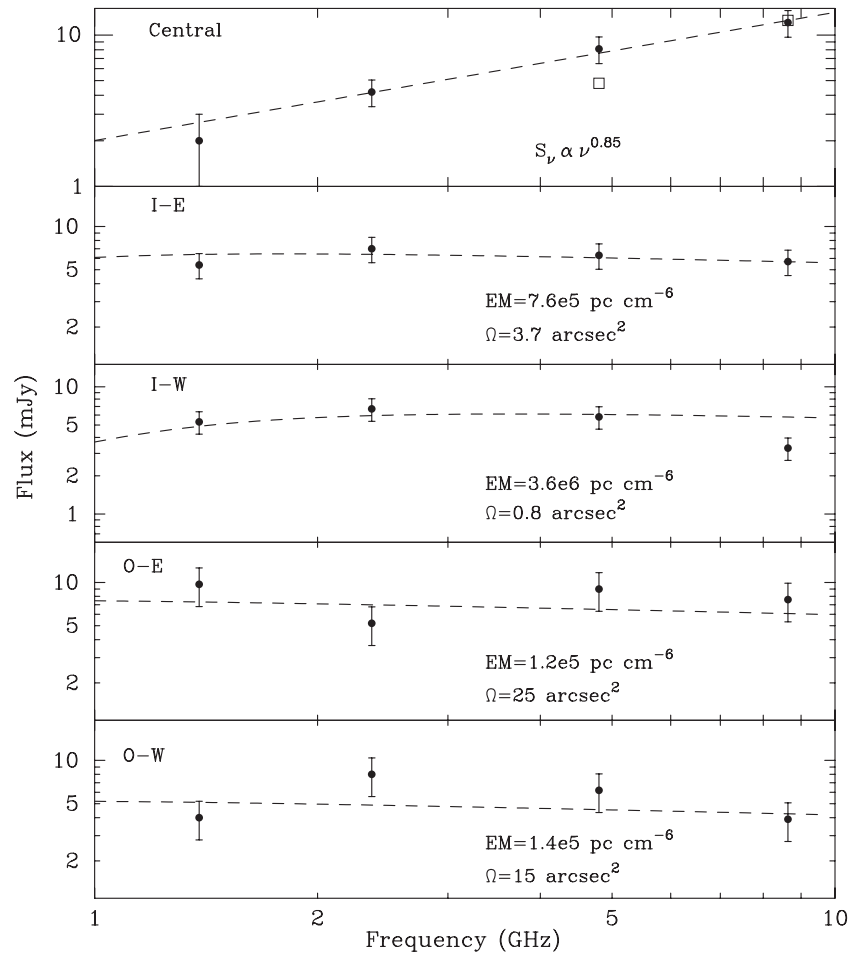
Figure 2. Radio continuum flux density vs. frequency for the five principal radio components detected toward IRAS 16562−3959. From top to bottom, spectra of the central, inner-east, inner-west, outer-east, and outer-west components. In the top panel, the dashed line indicates a least-squares power-law fit to the data. Empty squares represent the data reported by Urquhart et al. (2007). In the other panels, the dashed line indicates a least-squares fit to the observed spectra with a model of homogeneous region of ionized gas. The emission measure (EM) was fitted, and the solid angle (Ω) was obtained from the deconvolved size of the radio images at 8.6 GHz. Both parameters are given in each panel. Error bars are the maximum of either the error values in Table 1 or 20%.

Rodríguez et al. 2008), the constraint Equation (2) implies that the mass-loss rate is $\sim 1.4 \times 10^{-6}\ M_\odot\ \mathrm{yr}^{-1}$.

If the total luminosity of IRAS 16562−3959 is produced by a ZAMS star it would correspond to an O8 star, which emits a rate of ionizing photons of $2.2 \times 10^{48}\ \mathrm{s}^{-1}$ (Panagia 1973). Embedded in a constant density medium, this star would generate an H II region with a flux density of ~ 8.4 Jy at optically thin radio frequencies, far in excess of the observed value of ~ 10 mJy. We suggest that the weak radio emission from the central source is a consequence of IRAS 16562−3959 undergoing an intense accretion phase, with the central object still being in the pre-UC H II region sequence phase. The high-mass accretion rate of the infalling material forbids the development of a sizeable H II region (Yorke 1979; Walmsley 1995), and the free–free emission from the ionized material is considerably lowered at centimeter wavelengths.

The spectra of the radio emission from the lobes are rather flat, indicative of optically thin free–free emission. We suggest that the radio emission from the lobes arises in shocks resulting from the interaction of a collimated stellar wind with the surrounding medium. The dotted lines in Figure 2 correspond to fits of the observed spectra using a model of thermal emission from a homogeneous region of ionized gas. From these fits, we derive emission measures of $\sim 1 \times 10^6$ pc cm^{-6} toward the inner lobes and $\sim 1 \times 10^5$ pc cm^{-6} toward the outer lobes. For all lobes

the emission is optically thin within the range of observed frequencies. The solid angles were derived from the radio images giving 3.7, 0.8, 25, and 15 arcsec^2 for the inner-east, inner-west, outer-east, and outer-west lobes, respectively. The derived electron densities within the lobes are about $\sim 10^3$ cm^{-3} for the outer lobes and $\sim 10^4$ cm^{-3} for the inner lobes.

4.2. Characteristics of the Exciting Source and its Environment

The radio string is associated with a massive ($\sim 1.0 \times 10^3\ M_\odot$) and dense ($1.2 \times 10^6$ cm^{-3}) core detected at 250 GHz (1.2 mm) by Faúndez et al. (2004), with the central component offset from the millimeter continuum peak by $\sim 13''$, equivalent to 0.1 pc at 1.6 kpc.

Figure 3 shows that associated with the dust core there is strong diffuse K_s-band emission, centered near the central source and aligned along the jet axis. This emission extends $\sim 1\overset{.}{'}5$ in the east and west directions. There is also diffuse K_s-band emission arising from two regions located $\sim 3'$ toward the north and south of the central source. They are roughly symmetrically displaced from the central source but aligned in a perpendicular direction to the jet axis. The strong K_s-band emission is likely to be produced by excited H$_2$ 2.12 μm emission arising from shocked gas. Moreover, the arc-like morphology of the northern K_s-band emission feature located approximately at R.A. = 16^{h}59^{m}42^s, decl. = −40°00′13″ (J2000) is also
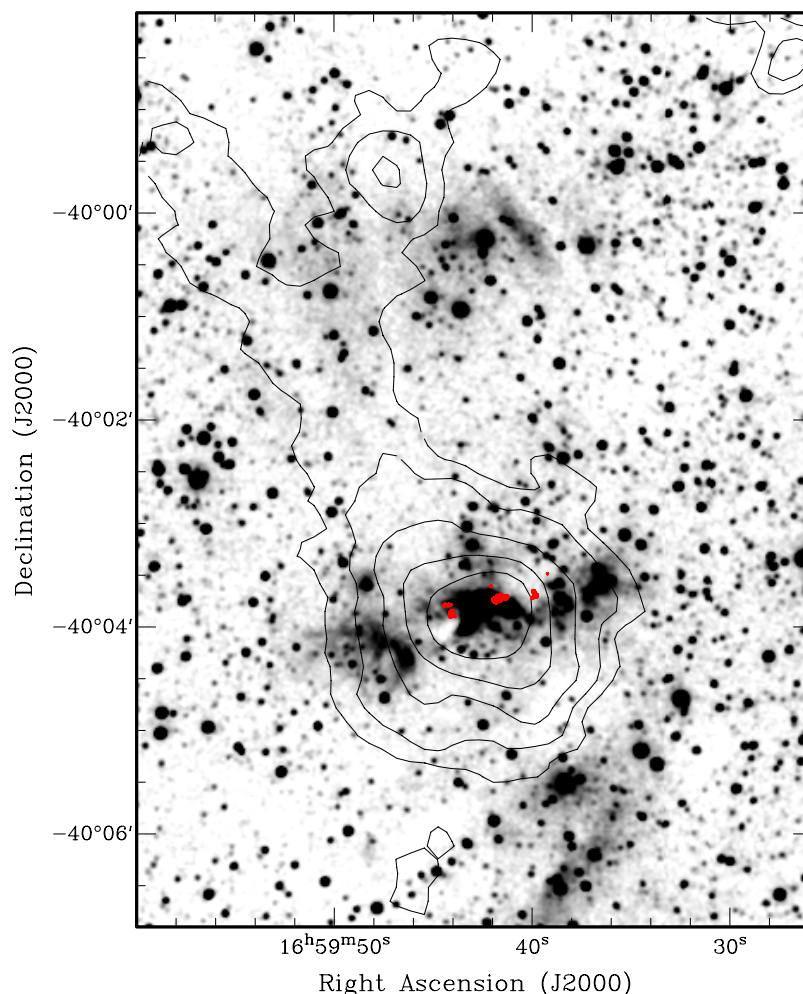
Figure 3. Gray scale image of the K_s-band emission toward IRAS 16562−3959. Black contours: 1.2 mm dust continuum emission (SIMBA/SEST). Red contours: 8.6 GHz radio continuum emission (ATCA).

consistent with HH phenomena. We note that the north–south structure is also seen as diffuse mid-infrared emission in the four *Midcourse Space Experiment* (*MSX*) bands (8.28, 12.13, 14.65, and 21.34 μm), indicating also a strong contribution from warm dust.

Figure 4 shows a zoom-in of the 8 μm emission from *Spitzer* and K_s-band emission from Two Micron All Sky Survey (2MASS) toward the central part of the core. There is an extended "V" shape feature extending along the east jet axis seen in both K_s band and 8 μm. In addition, there are three OH masers (Caswell 1998, 2004): one is associated with the central source, the second is associated with an 8 μm source, unseen in 2MASS, located ∼15″ northeast of the central source, and the third is located close to the east jet axis at about 2″ from the outer-east lobe. Their velocities are close to the radial velocity of the ambient cloud ($V_{LSR} = -12.6$ km s^{-1}; Urquhart et al. 2008b), except for the eastern OH maser, which has a radial velocity of −24.5 km s^{-1}. Infrared continuum emission at 10.4 μm is shown in Figure 5, which displays an image[5] obtained with TIMMI2 by Mottram et al. (2007). It shows intense emission associated with the central source and more diffuse emission associated with the inner-east radio lobe. There is also an extended 4.5 μm emission enhancement associated with the central source (see Figure 6). These "green fuzzies,"

seen as green in a three-color IRAC image, have been related to shocked gas in protostellar environments (Chambers et al. 2009). All of the phenomena described above are readily associated with high-mass star formation and therefore support the notion that IRAS 16562−3959 is a high-mass young stellar object with an energetic outflow activity.

While the east–west K_s-band structure can be related directly to the radio jet, the identification of the energy source of the north–south K_s-band feature is less clear. One possibility is that the north–south feature is driven by the central jet source, which will imply a re-orientation of the jet in almost 90°. Models of close stellar encounters do not, however, predict such large precession of the outflow axis (e.g., Moeckel & Bally 2006), and thus this possibility appears unlikely. Since MYSOs are known to be formed in clusters, the most plausible explanation is that a yet unidentified nearby source is the exciting source of the north–south K_s-band emission. A possible candidate is the YSO, located 16″ northeast of the central component, identified from the *Spitzer* data. As pointed out previously, this object is associated with an OH maser with a radial velocity similar to that of the ambient cloud. This and the central source thus belong to the same star-forming region, as suggested by Caswell (1998).

Figure 7 shows the SED of IRAS 16562−3959 from 3.6 to 1200 μm, including flux densities at 1.2 mm (Faúndez et al. 2004); at 12, 25, 60, and 100 μm obtained from the
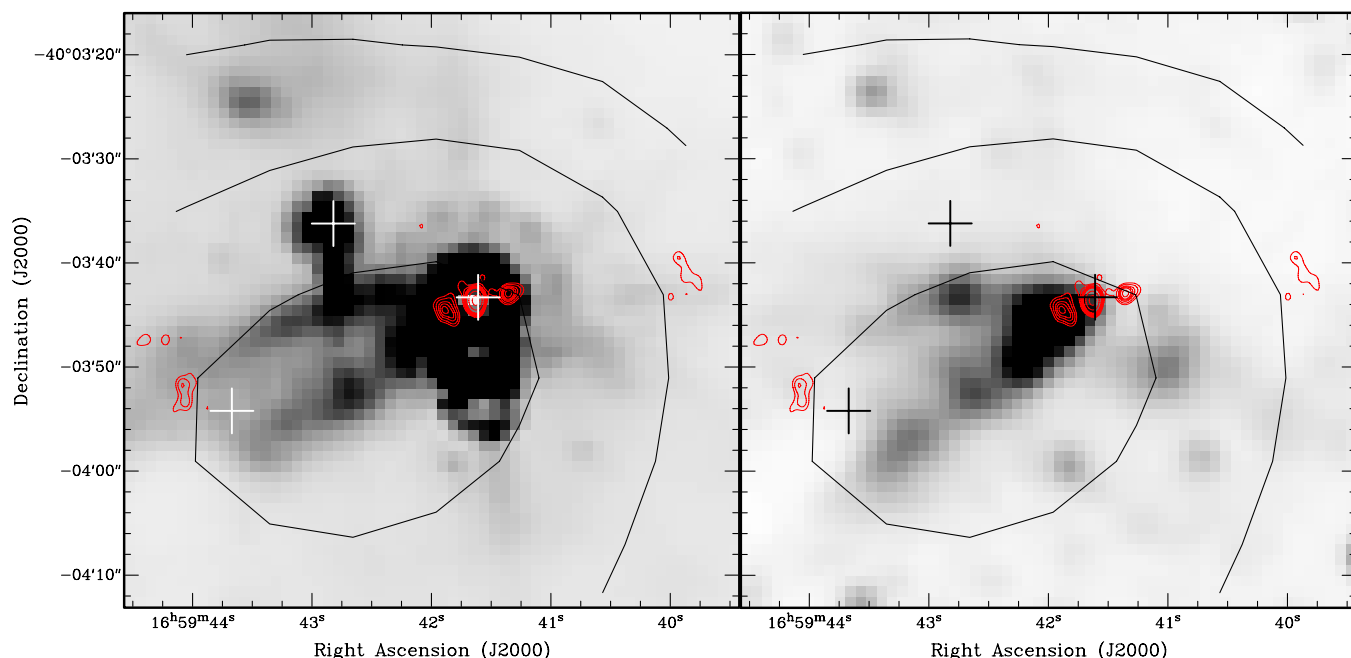
Figure 4. Left—gray image: 8 μm IRAC-*Spitzer* emission. Black contours: 250 GHz dust emission detected with SIMBA. Red contours: 8.6 GHz emission. Crosses mark the position of the OH masers. Note that the 8 μm data are saturated near the central source, which produces an spurious extension running toward the south. Right—gray image: K_s-band emission. Contours and symbols are the same as in the left panel.
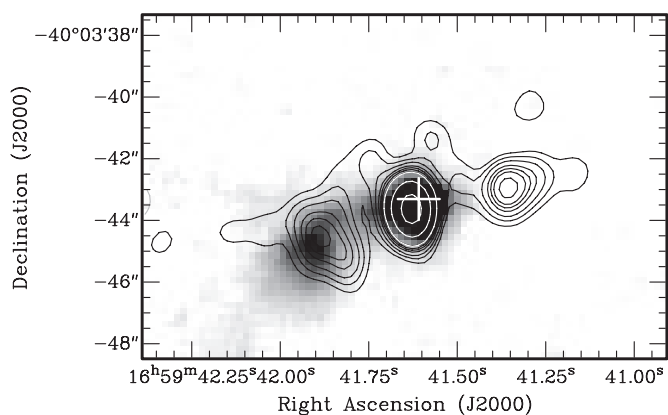

Figure 5. Gray scale: TIMMI2 10.4 μm emission. Contours: 8.6 GHz radio emission. The cross marks the position of the OH maser associated with the central source. There is a strong 10.4 μm emission associated with the central source and more diffuse emission associated with the inner-east lobe.

Figure 6. *Spitzer* three-color image using the 8.0 μm, 4.5 μm, and 3.6 μm IRAC images for red, green, and blue, respectively. The jet is located at the center of the image associated with an extended diffuse "green fuzzy" or enhancement of the 4.5 μm band.

IRAS database; at 8.3, 12.1, 14.7, and 21.3 μm obtained from the *MSX* Survey of the Galactic Plane database (Price et al. 2001; *MSX* source G345.4938+01.4677); and at 3.6 and 4.5 μm obtained from *Spitzer*-IRAC images using an aperture of ∼1′. The IRAC images at 5.8 and 8.0 μm data were saturated and an adequate flux estimation was not possible. In the frequency range covered by the SED, the emission is mainly due to thermal dust emission. The SED was analyzed by fitting model SEDs using a large grid of precomputed models (Robitaille et al. 2007). The continuous line in Figure 7 presents the result of the best fit. The derived parameters from the fit are given in Table 2. The SED fitting indicates that the energy source corresponds to a deeply embedded YSO, and rules out the possibility of being a heavily extincted star.

The mass of the host envelope derived from the fitting is ∼1700 $M_\odot$. However, the model of Robitaille et al. (2007)

Table 2
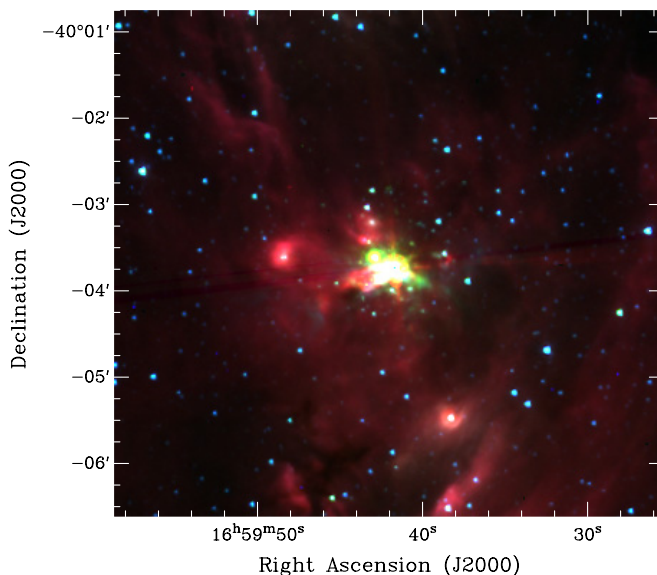SED Fitting

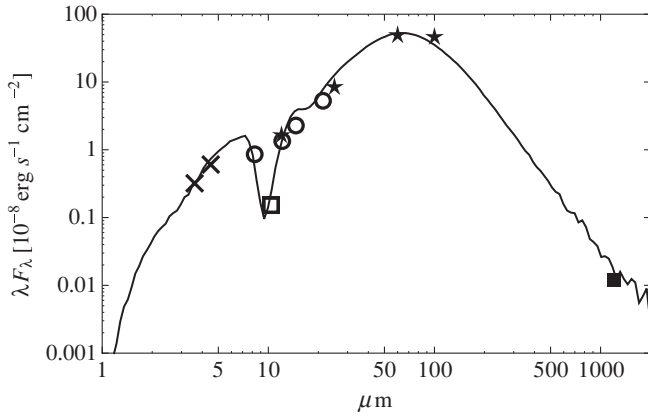| Parameter	Value
Inclination	41°
Stellar age	4.5×10^4 yr
Stellar mass	14.7 $M_\odot$
Envelope accretion rate	3.4×10^{-3} $M_\odot$ yr^{-1}
Disk mass	0.26 $M_\odot$
Disk accretion rate	5.5×10^{-4} $M_\odot$ yr^{-1}
Total luminosity	5.8×10^4 $L_\odot$
Envelope mass	1.7×10^3 $M_\odot$

Figure 7. SED of the central source. Crosses: *Spitzer/IRAC* data at 3.6 and 4.5 μm. Empty square: TIMMI2 data at 10.4 μm. Empty circles: *MSX* data at 8.3, 12.1, 14.7, and 21.3 μm. Stars: *IRAS* data at 12, 25, 60, and 100 μm. Filled square: SIMBA data at 1200 μm. The line indicates the best fit using the models described in Robitaille et al. (2007).

does not consider the increase of absorption at millimeter frequencies due to ice coatings in the dust grains (Ossenkopf & Henning 1994) and in consequence is probably overestimating the mass of the envelope by a factor of 2–3. Therefore, the mass of the core derived from the 1.2 mm observations of 910 $M_\odot$ is in fair agreement with the SED fitting. We note that Faúndez et al. (2004) reported a mass of 1500 $M_\odot$, but a new analysis of the data shows that for this particular source an erroneous calibration factor was applied, which produced an overestimation of the flux by a factor of 1.76 (López et al. 2010).

The fitting also indicates that the central YSO has a mass of $\sim 15\ M_\odot$ and a luminosity of $5.8 \times 10^4\ L_\odot$, that the envelope is undergoing an intense accretion phase with a rate of $3.4 \times 10^{-3}\ M_\odot\ \mathrm{yr}^{-1}$, and that the accretion rate onto the central object is $5.5 \times 10^{-4}\ M_\odot\ \mathrm{yr}^{-1}$. The derived stellar parameters are similar to those of a B0 $\sim$ O9.5 main-sequence star (Sternberg et al. 2003) and an O8.5 ZAMS star (Panagia 1973). We also note that the derived infall accretion rate is greater than $\sim 1.0 \times 10^{-5}\ M_\odot\ \mathrm{yr}^{-1}$, the infall rate needed to quench the development of a sizeable H II region (Walmsley 1995).

The linear morphology and spectral characteristics of the radio sources suggest that the string is physically associated with a highly collimated wind arising from a young, MYSO with the lobes tracing the interaction between the jet and the ambient cloud. We postulate that the lobes radio emission corresponds to thermal emission coming from shocked ionized gas situated in the working surfaces of the central jet source. Particularly, we rule out the possibility that the radio emission has an extragalactic origin—the probability of finding an extragalactic source at 5 GHz with a flux density above 5 mJy within 20″ from the peak of the 1.2 mm dust emission is 3.5×10^{-4} (Fomalont et al. 1991).

4.3. Jet and Shock Parameters

In this section, we make use of the observed quantities of the lobe emission to derive parameters of the jet–ambient medium interaction. Considering that the free–free emission from the lobes arises from a shock wave formed at the head of the jet, the emission measure (EM) is given in terms of shock parameters

by (Curiel et al. 1993)

$$\left(\frac{\mathrm{EM}}{10^6\ \mathrm{pc\ cm^{-6}}} \right) = 1.39 \left(\frac{n_a}{10^5\ \mathrm{cm^{-3}}} \right) \left(\frac{V_s}{100\ \mathrm{km\ s^{-1}}} \right)^{1.68}$$
$$\times \left(\frac{T_e}{10^4\ \mathrm{K}} \right)^{0.8}, \tag{3}$$

where n_a, V_s, and T_e are the particle ambient density, the shock velocity, and the temperature of the shock-ionized gas. If the ambient density is known, this expression can be used to estimate the shock velocity.

To estimate the ambient density at the position of the lobes, we re-analyzed the 1.2 mm data taken by Faúndez et al. toward IRAS 16562−3959 and fitted the observed radial intensity profiles from the core region using a model in which the density and temperature follow power-law radial distributions (Adams 1991). The best fit to the image was obtained with the following molecular gas density and temperature profiles: $n_a(r) = n_0(0.1\ \mathrm{pc}/r)^{1.9}$ and $T(r) = T_0(0.1\ \mathrm{pc}/r)^{0.4}$, where $n_0 = 1.4 \times 10^5\ \mathrm{cm^{-3}}$ and $T_0 = 50$ K. We assumed a gas-to-dust mass ratio of 100 and a mean molecular mass of 2.3 m_H. The derived density profile implies that the mass of the core, within a radius of $\sim 90''$, is 790 $M_\odot$, and that the ambient density at the position of the east and west inner lobes—displaced from the core center by 10″ and 18″—are 2.3×10^5 and $7.6 \times 10^4\ \mathrm{cm^{-3}}$, respectively. Using these densities and the emission measures computed in Section 3, we derive from Equation (3) that the shock velocities at the east and west inner lobes are 119 and 91 km s^{-1}, respectively. The same analysis applied to the east and west outer lobes gives shock velocities of ~ 24 and ~ 66 km s^{-1}, respectively, consistent with the expectation that shock velocity should decrease away from the jet source.

Assuming a simple one-dimensional isothermal shock model (e.g., Masson & Chernin 1993) and that the momentum flux imparted to the shock ionized material by the jet equals the ram pressure of the ambient material, then

$$(V_j - V_s)^2 \rho_j = V_s^2 \rho_a, \tag{4}$$

where ρ_j and V_j are the mass density and velocity of the jet, respectively, and ρ_a is the ambient gas mass density. If the shock velocity, ambient density, and jet density are known, this expression can be used to estimate the jet velocity. The density of the jet at the positions of the inner lobes can be estimated from Equation (1). The lobes are displaced from the jet by 3″, which translates into a physical distance of 0.033 pc, assuming an inclination of 45°. Using $\theta = 0.2$ and assuming $v_m = 10$ GHz, the density of the jet at 0.033 pc is $1.2 \times 10^{-19}\ \mathrm{g\ cm^{-3}}$, about ~ 4 times lower than the ambient density. Using the values derived for the east and west inner lobes of the shock velocity, ambient density, and jet density, we determine from Equation (4) jet velocities of 360 and 280 km s^{-1}, respectively.

We further estimate that the most recent ejection, giving rise to the inner lobes, took place between 90 and 120 years ago. Moreover, from Equation (2) and taking again 10 GHz as the turnover frequency, we derive mass-loss rates of 1.0 and $0.79 \times 10^{-6}\ M_\odot\ \mathrm{yr}^{-1}$, which in combination with the ejecta velocities give momentum rates of 3.7×10^{-4} and $2.2 \times 10^{-4}\ M_\odot\ \mathrm{km\ s^{-1}\ yr^{-1}}$ for the east and west halves of the bipolar jet, respectively.

5. SUMMARY

We made radio continuum observations at 1.4, 2.4, 4.8, and 8.6 GHz, using ATCA, toward IRAS 16562−3959, a luminous

object ($L \sim 7 \times 10^4\,L_\odot$) thought to be a massive star-forming region in an early stage of evolution. The main results and conclusions are summarized as follows.

1. The radio continuum observations show the presence of a remarkable string of radio emission, consisting of a compact, bright central component, two inner lobes, separated by about $7''$ and symmetrically located from the central source, and two outer lobes, separated by about $45''$.

2. The emission from the central object has a spectral index between 1.4 and 8.6 GHz of 0.85 ± 0.15, consistent with free–free emission from a thermal jet. Assuming that the jet corresponds to a bipolar pressure-confined wind with an aperture angle $\theta = 0.2$, we estimate that the jet has a total mass-loss rate of $\sim 2 \times 10^{-6}\,M_\odot\,\mathrm{yr}^{-1}$.

3. The radio emission from the lobes has spectral indices of typically -0.1, characteristic of thermal emission. We suggest that the emission from the lobes arises in shocks resulting from the interaction of a collimated wind with the surrounding medium.

4. The string is found projected toward a massive and dense core and associated with several indicators of massive star formation and shock gas tracers. The jet is located near the peak position of the dust emission. We conclude that the massive core hosts a high-mass star in an early stage of evolution in which it is undergoing the ejection of a powerful collimated stellar wind, showing that jets found in the formation of low-mass stars are also produced in high-mass stars.

REFERENCES

Adams, F. C. 1991, ApJ, 382, 544
Anglada, G. 1996, in ASP Conf. Ser. 93, Radio Emission from the Stars and the Sun, ed. A. R. Taylor & J. M. Paredes (San Francisco, CA: ASP), 3
Beuther, H., & Walsh, A. J. 2008, ApJ, 673, L55
Bronfman, L., Garay, G., Merello, M., Mardones, D., May, J., Brooks, K. J., Nyman, L.-Å., & Güsten, R. 2008, ApJ, 672, 391
Brooks, K. J., Garay, G., Voronkov, M., & Rodríguez, L. F. 2007, ApJ, 669, 459
Casoli, F., Combes, F., Dupraz, C., Gerin, M., & Boulanger, F. 1986, A&A, 169, 281
Caswell, J. L. 1998, MNRAS, 297, 215
Caswell, J. L. 2004, MNRAS, 349, 99
Cesaroni, R., Felli, M., Testi, L., Walmsley, C. M., & Olmi, L. 1997, A&A, 325, 725
Chambers, E. T., Jackson, J. M., Rathborne, J. M., & Simon, R. 2009, ApJS, 181, 360
Curiel, S., Rodriguez, L. F., Moran, J. M., & Canto, J. 1993, ApJ, 415, 191
Curiel, S., et al. 2006, ApJ, 638, 878
Devine, D., Bally, J., Reipurth, B., Shepherd, D., & Watson, A. 1999, AJ, 117, 2919
Faúndez, S., Bronfman, L., Garay, G., Chini, R., Nyman, L.-Å., & May, J. 2004, A&A, 426, 97
Fomalont, E. B., Windhorst, R. A., Kristian, J. A., & Kellerman, K. I. 1991, AJ, 102, 1258
Garay, G., Brooks, K. J., Mardones, D., & Norris, R. P. 2003, ApJ, 587, 739
Hoare, M. G., Kurtz, S. E., Lizano, S., Keto, E., & Hofner, P. 2007, in Protostars and Planets V, ed. B. Reipurth, D. Jewitt, & K. Keil (Tucson, AZ: Univ. Arizona Press), 181
López, C., Bronfman, L., Nyman, L.-Å., May, J., & Garay, G. 2010, A&A, submitted
Martí, J., Rodríguez, L. F., & Reipurth, B. 1993, ApJ, 416, 208
Martí, J., Rodríguez, L. F., & Reipurth, B. 1998, ApJ, 502, 337
Masson, C. R., & Chernin, L. M. 1993, ApJ, 414, 230
Moeckel, N., & Bally, J. 2006, ApJ, 653, 437
Mottram, J. C., Hoare, M. G., Lumsden, S. L., Oudmaijer, R. D., Urquhart, J. S., Sheret, T. L., Clarke, A. J., & Allsopp, J. 2007, A&A, 476, 1019
Ossenkopf, V., & Henning, T. 1994, A&A, 291, 943
Panagia, N. 1973, AJ, 78, 929
Price, S. D., Egan, M. P., Carey, S. J., Mizuno, D. R., & Kuchar, T. A. 2001, AJ, 121, 2819
Reynolds, S. P. 1986, ApJ, 304, 713
Robitaille, T. P., Whitney, B. A., Indebetouw, R., & Wood, K. 2007, ApJS, 169, 328
Rodríguez, L. F., Garay, G., Brooks, K. J., & Mardones, D. 2005, ApJ, 626, 953
Rodríguez, L. F., Garay, G., Curiel, S., Ramírez, S., Torrelles, J. M., Gómez, Y., & Velazquez, A. 1994, ApJ, 430, L65
Rodríguez, L. F., Moran, J. M., Franco-Hernández, R., Garay, G., Brooks, K. J., & Mardones, D. 2008, AJ, 135, 2370
Sault, R. J., Teuben, P. J., & Wright, M. C. H. 1995, in ASP Conf. Ser. 77, Astronomical Data Analysis Software and Systems IV, ed. R. A. Shaw, H. E. Payne, & J. J. E. Hayes (San Francisco, CA: ASP), 433
Shepherd, D. S., Claussen, M. J., & Kurtz, S. E. 2001, Science, 292, 1513
Shepherd, D. S., Testi, L., & Stark, D. P. 2003, ApJ, 584, 882
Shepherd, D. S., Watson, A. M., Sargent, A. I., & Churchwell, E. 1998, ApJ, 507, 861
Sternberg, A., Hoffmann, T. L., & Pauldrach, A. W. A. 2003, ApJ, 599, 1333
Urquhart, J. S., Busfield, A. L., Hoare, M. G., Lumsden, S. L., Clarke, A. J., Moore, T. J. T., Mottram, J. C., & Oudmaijer, R. D. 2007, A&A, 461, 11
Urquhart, J. S., Hoare, M. G., Lumsden, S. L., Oudmaijer, R. D., & Moore, T. J. T. 2008a, in ASP Conf. Ser. 387, Massive Star Formation: Observations Confront Theory, ed. H. Beuther, H. Linz, & T. Henning (San Francisco, CA: ASP), 381
Urquhart, J. S., et al. 2008b, A&A, 487, 253
Walmsley, M. 1995, Rev. Mex. Astron. Astrofis. Ser. Conf., 1, 137
Yorke, H. W. 1979, A&A, 80, 308